THE JOURNAL OF PHYSICAL CHEMISTRY C

Article

pubs.acs.org/JPCC

Surface Structure of TiO_2 Rutile (011) Exposed to Liquid Water

Jan Balajka,[†] Ulrich Aschauer,[‡] Stijn F. L. Mertens,[†] Annabella Selloni,[§] Michael Schmid,[†] and Ulrike Diebold*[,†]

[†]Institute of Applied Physics, TU Wien, Wiedner Hauptstraße 8-10/134, 1040 Vienna, Austria

[‡]Department of Chemistry and Biochemistry, University of Bern, Freiestrasse 3, CH-3012, Bern, Switzerland

[§]Department of Chemistry, Princeton University, Frick Laboratory, Princeton, New Jersey 08544, United States

Supporting Information

ABSTRACT: The rutile TiO_2(011) surface exhibits a (2 × 1) reconstruction when prepared by standard techniques in ultrahigh vacuum (UHV). Here we report that a restructuring occurs upon exposing the surface to liquid water at room temperature. The experiment was performed in a dedicated UHV system, equipped for direct and clean transfer of samples between UHV and liquid environment. After exposure to liquid water, an overlayer with a (2 × 1) symmetry was observed containing two dissociated water molecules per unit cell. The two OH groups yield an apparent "c(2 × 1)" symmetry in scanning tunneling microscopy (STM) images. On the basis of STM analysis and density functional theory (DFT) calculations, this overlayer is attributed to dissociated water on top of the unreconstructed (1 × 1) surface. Investigation of possible adsorption structures and analysis of the domain boundaries in this structure provide strong evidence that the original (2 × 1) reconstruction is lifted. Unlike the (2 × 1) reconstruction, the (1 × 1) surface has an appropriate density and symmetry of adsorption sites. The possibility of contaminant-induced restructuring was excluded based on X-ray photoelectron spectroscopy (XPS) and low-energy He^+ ion scattering (LEIS) measurements.

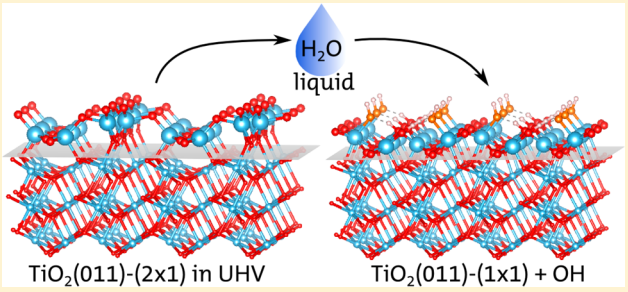

INTRODUCTION

Many technologically important processes take place at the interface between solid and aqueous solutions. Knowledge of the interfacial structure is therefore essential in order to understand, control, and potentially improve the processes. The interaction of water with solid surfaces has been widely studied on different classes of materials.[1−3] While the structure of the first water layer on metals is understood to a significant extent,[4−6] interaction of water with oxides is generally more complex as both surface metal and oxygen atoms can act as H-binding sites.[7,8]

Titanium dioxide (TiO_2) is a prototypical metal oxide,[9] and most of its numerous applications involve liquid water on the surface such as in photocatalytic water splitting. While the interaction of low-pressure gas-phase water with TiO_2 has been studied extensively, studies of the liquid water−TiO_2 interface are scarce. Recently, the interaction of liquid water with TiO_2(110), the predominant rutile surface, has been studied by exposing the surface to humid environment and subsequently characterizing it in ultrahigh vacuum (UHV)[10−12] or directly by STM in liquid.[13,14] Here we report on the interfacial structure between the less-investigated (011) surface of TiO_2 rutile and liquid water. This surface is the second-lowest energy termination of TiO_2 rutile and constitutes a sizable fraction of equilibrium-shape nanoparticles.[15] In addition, a difference in photocatalytic activity of the (011) surface with respect to the (110) has been reported.[16]

The (011) surface exhibits a (2 × 1) reconstruction when prepared in UHV. The "brookite (001)-like" model of the (2 × 1) reconstruction was proposed on the basis of STM and surface X-ray diffraction (SXRD) measurements and DFT calculations.[17,18] According to DFT predictions,[19] the (2 × 1) reconstruction is no longer favorable in a liquid-water environment and deconstructs to the bulk-terminated (1 × 1) structure. It has in fact been proposed recently[20] that the surface structure of titania and metal oxides is in general different from the structure known in UHV in the presence of adsorbates. For example, the ability of the (011) surface to reversibly change its structure in response to adsorbed molecules of acetic acid has been demonstrated in ref 21.

In this study we interface the TiO_2(011)-(2 × 1) surface with liquid water in order to approach application-relevant conditions, while performing the experiments in a highly controlled manner to avoid contamination-induced artifacts and enable interpretation of the results. Our experimental results show that the (2 × 1) reconstruction of the TiO_2(011) surface is lifted in accordance with the DFT predictions,[19] and an ordered array of surface hydroxyls with apparent higher symmetry remains on top of the (1 × 1) surface when the sample is reintroduced to UHV.

Received: September 29, 2017
Revised: October 27, 2017
Published: October 31, 2017

DOI: 10.1021/acs.jpcc.7b09674
J. Phys. Chem. C 2017, 121, 26424−26431

METHODS

Experimental Details. The experiments were performed in a UHV chamber with a base pressure of 1×10^{-10} mbar equipped with STM, XPS, LEIS, low-energy electron diffraction (LEED), and a separately pumped load lock.

The sample was mounted on a Mo Omicron-type sample holder with Ta clips. The TiO_2 rutile (011) sample (MTI Corp., one side polished) was prepared by cycles of Ar^+ ion sputtering (1 keV, 0.6 $\mu A/cm^2$, 20 min) with a rastered ion source (SPECS, IQE 12/38) and radiative annealing up to 680 °C. The temperature was measured with a K-type thermocouple spot-welded on the sample-holder clamp and independently verified by an infrared pyrometer (LumaSense Impac IGA 140, emissivity 77%). The purity of gases (Ar, He, O_2) was checked with a quadrupole mass spectrometer (SRS RGA 100). Formic acid (HCOOH, Sigma-Aldrich, purity 98%) for the C 1s reference measurement on TiO_2 rutile (110) was cleaned by several freeze−pump−thaw cycles and purity checked with the RGA prior to dosing.

The STM images were acquired with an Omicron UHV STM-1 at room temperature in constant-current mode with positive sample bias (imaging empty states). The sample bias and tunneling current are indicated in each STM image. For STM tips electrochemically etched W wire (0.5 mm) was used, cleaned by Ar^+ sputtering, and conditioned *in situ* by applying voltage pulses. Fourier transforms of STM images were obtained from images corrected for distortions.[22] XPS measurements were conducted with a dual-anode X-ray source (Mg Kα and Al Kα) and a SPECS PHOIBOS 100 analyzer at both normal emission (0° from the surface normal) and grazing emission (60° from the surface normal) with a pass energy of 20 eV. Overview scans were acquired with a pass energy of 60 eV. In LEIS measurements an incident beam of He^+ ions with 1225 eV kinetic energy was scattered at an angle of 137° and detected with the same hemispherical analyzer at a pass energy of 110 eV. The background He pressure was 5×10^{-8} mbar, and the sample current was 10 nA. The ion beam was not rastered during LEIS measurements but stationary on one place. A few spectra on different places of the sample were acquired and averaged. For low-energy electron diffraction (LEED) an Omicron SPECTALEED was used at electron energies denoted in the figures. A dark frame (zero screen voltage) and flat field (LEED image of the polycrystalline sample holder at the same energy) were acquired and used for correcting the LEED images for inhomogeneous illumination, screen, and camera artifacts.

A typical experiment proceeded in the following way: The sample was prepared by sputtering and annealing cycles and characterized in UHV prior to exposing it to liquid water. Then the sample was brought to the load lock (base pressure 1×10^{-9} mbar), which was then separated from the main chamber and vented with argon (99.999% purity, additionally purified with an in-line sorption filter MC50-902 FV from SAES). The load lock was then opened in order to dose a small drop (volume 20 μL) of fresh, ultrapure H_2O (Milli-Q, Millipore, 18.2 MΩ·cm, ≤3 ppb total organic carbon) using a pipet (Eppendorf). The water droplet spread on the hydrophilic surface forming a thin layer of liquid water. Emphasis was placed on minimizing the time of the sample exposure to Ar at atmospheric pressure (typically <10 s). During that time, a slight argon overpressure was maintained inside the load lock. Some backstreaming of the air in the argon flow is assumed to be responsible for the small carbon peak observed by XPS. The wet sample was then brought back into the load lock and immediately evacuated using a liquid-nitrogen-cooled sorption pump (Ultek, PerkinElmer). In the case of a small droplet (as used in the present study) the liquid water evaporated immediately after opening the pump. In the case of bigger drops the liquid water went through the triple point due to the sudden pressure drop, transiently boiling and freezing at the same time. The frozen flake on the sample surface then slowly sublimed.

After ca. 1 min of pumping the pressure reached 1×10^{-2} mbar, and the load lock was opened to a turbomolecular pump running at full speed behind a gate valve. Within 5−10 min the load lock was evacuated to 1×10^{-6} mbar, which allowed transfer into the main chamber (1×10^{-10} mbar) for analysis. The sample was then characterized with STM, XPS, LEIS, and LEED, in this order to minimize ion- or electron-beam-damage artifacts.

Computational Details. The density functional theory (DFT) calculations were performed within the plane-wave/pseudopotential formalism as implemented in the Quantum ESPRESSO package[23] using the Perdew−Burke−Ernzerhof (PBE) exchange-correlation functional.[24] Wave functions were expanded in plane waves up to a kinetic energy of 25 Ry together with a cutoff of 200 Ry for the augmented density, and reciprocal space was sampled using a $1 \times 2 \times 1$ mesh. Ultrasoft pseudopotentials[25] included Ti(3s, 3p, 3d, 4s), O(2s, 2p), and H(1s) valence states. The surface was represented by a four layer thick slab with in-plane dimensions of 9.213 Å × 5.461 Å and a 10 Å vacuum gap along the surface-normal direction. Structural relaxations were carried out until forces converged below 0.05 eV/Å. Atoms belonging to the bottom-most TiO_2 layer were kept fixed at their bulk position. STM images were computed in constant-density mode using the Tersoff−Hamann approach.[26] Born−Oppenheimer molecular dynamics at 300 K starting from the relaxed structures were performed to account for the thermal motion of the adsorbed OH groups in STM images. Following 0.97 ps of equilibration, STM images were computed every 0.0097 ps over 4 ps. These data sets were then averaged to obtain STM images with finite-temperature effects.

RESULTS

Experimental Results. *TiO_2 Rutile (011): UHV-Prepared Surface.* The TiO_2 rutile (011)-(2 × 1) surface was prepared by sputtering and annealing in UHV. The typical appearance in STM is shown in Figure 1a. Bright zigzag rows run along the $[01\bar{1}]$ direction with dark rows in between these, corresponding to ridges and valleys of the (2 × 1) reconstruction. Figure 1d shows the calculated, fully relaxed structure and a simulated STM image for the reconstructed (2 × 1) termination. The typical zigzag rows agree well with experimental STM images recorded in UHV (Figure 1a). The STM contrast depends strongly on the tunneling conditions.[18,27] The additional, brighter features originate from residual water adsorption in the UHV chamber, most likely via water dissociation on O vacancies that result from standard UHV preparation procedures. Here the density of adsorbed residual water is relatively high as the image was acquired ca. 7 h after preparation. The fast Fourier transform (FFT) in Figure 1b shows a (2 × 1) reciprocal lattice, as does LEED in Figure 1c. The $(0, 2n - 1)$ spots in the Fourier transform of the STM

DOI: 10.1021/acs.jpcc.7b09674
J. Phys. Chem. C 2017, 121, 26424−26431

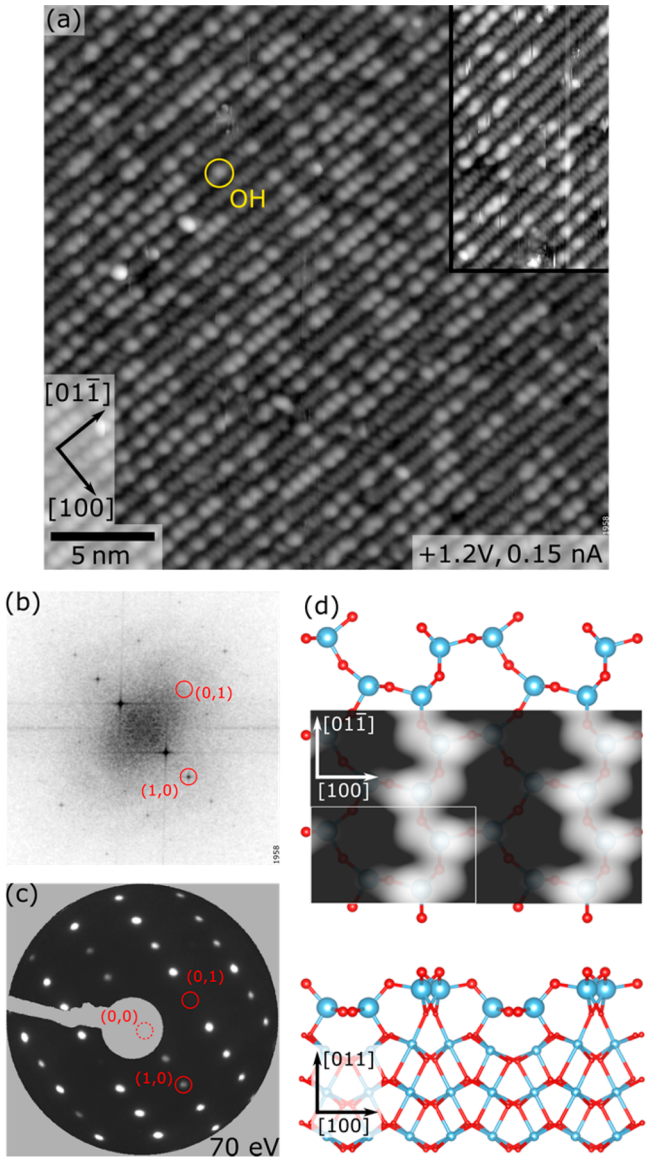

Figure 1. UHV-prepared TiO_2 rutile (011)-2 × 1 surface: (a) STM (inset: higher resolution), (b) FFT, and (c) LEED. The (0, 2n − 1) spots in FFT and LEED are missing due to a glide-plane symmetry. (d) Computed structure (top and side views) and simulated STM image of the (2 × 1) reconstructed surface.

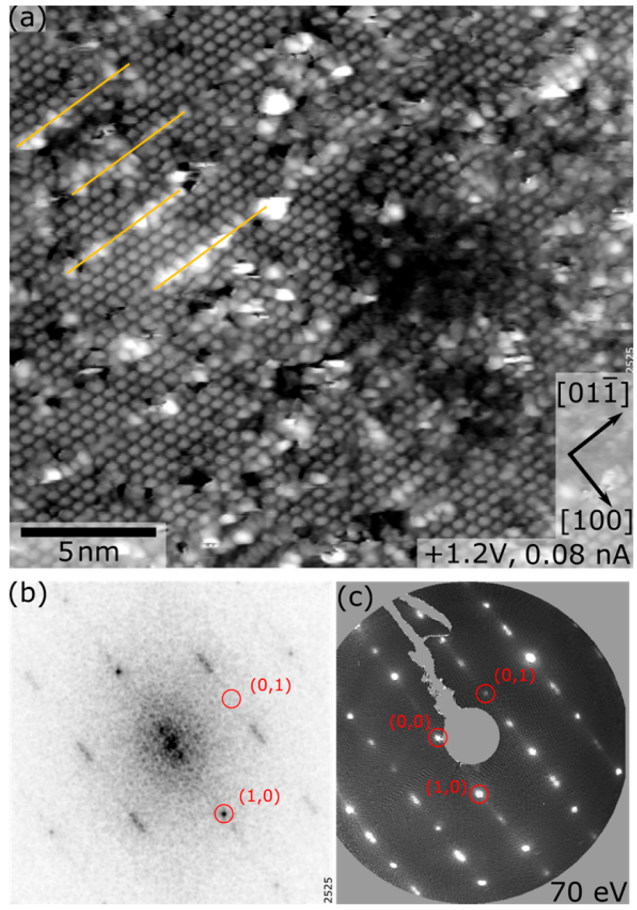

Figure 2. TiO_2 rutile (011) surface after contact with liquid water (a) STM, (b) FFT of (a), and (c) LEED. An overlayer of dissociated water with (2 × 1) symmetry on top of the unreconstructed (1 × 1) surface is imaged by STM with apparent "c(2 × 1)" symmetry, while LEED shows a (2 × 1) pattern (c). The splitting of some spots is a consequence of antiphase domains within the overlayer. Domain boundaries are highlighted with yellow lines.

image and in the LEED pattern, where n is an integer number, are missing due to a glide plane symmetry of the lattice.

TiO_2 Rutile (011): Surface after Exposure to Liquid H_2O. After the (2 × 1) surface was exposed to liquid water and transferred back into the UHV chamber, it was first characterized with STM to exclude the possibility of beam damage by other techniques (mainly LEIS and LEED). The STM image in Figure 2a shows that the (2 × 1) reconstruction is not retained after contact with liquid water. Instead, an ordered array with an apparent "c(2 × 1)" symmetry with respect to the bulk-terminated (1 × 1) surface is observed. This pseudohexagonal arrangement can also be viewed as the (1 × 1) structure with every other row shifted by half a unit-cell distance in the [01$\bar{1}$] direction. The FFT pattern in Figure 2b corresponds to the reciprocal lattice of such a "c(2 × 1)" structure. It can be described as a (2 × 1) reciprocal pattern (Figure 1b) with extinctions alternatingly at fractional and integral order spots. Half of the spots of the (2 × 1) pattern are extinct, namely those with indices (h, k), that satisfy the condition $h + 1/2k = n + 1/2$, where n is an integer. Contrary to STM, LEED shows all spots of the (2 × 1) pattern (Figure 2c). Here, because of mechanical constraints, the sample normal was not aligned perpendicular to the LEED screen, and therefore the (0,0) spot of the pattern is not at the center. Because of nonperpendicular incidence of the electron beam, the glide plane symmetry is broken and (0, 2n − 1) spots are only attenuated but do not vanish completely.

STM also shows domain boundaries running along the [01$\bar{1}$] direction, visible as brighter rows in Figure 2a. The two domains at either side appear to be shifted with respect to each other by half a unit cell along the boundary. The existence of antiphase domains on the surface is manifested by the elongation and splitting of some of the FFT and LEED spots. The spot splitting occurs only at fractional spots both in FFT and LEED (Figure 2b,c). In the FFT of the STM image, half of the fractional spots (h, k), where k is an even number, are completely missing due to the apparent higher symmetry of the lattice. Some of the half-order spots in LEED (Figure 2b) do not show such a clear splitting at this electron beam energy (70 eV). For example, the (1/2, 1) spot appears to be single

DOI: 10.1021/acs.jpcc.7b09674
J. Phys. Chem. C 2017, 121, 26424−26431

while at different energies it is split (see Supporting Information for a LEED pattern at 50 eV beam energy).

In some parts of the crystal, small areas of the (2 × 1) reconstruction were still present even after the contact with liquid water. Such reconstructed area is part of the STM image in Figure 3 and allows us to analyze how the new "c(2 × 1)" structure connects to the original (2 × 1) reconstruction. Alternating rows of the "c(2 × 1)" structure are in line with the ridges (bright zigzag) and valleys (dark) of the (2 × 1) reconstruction.

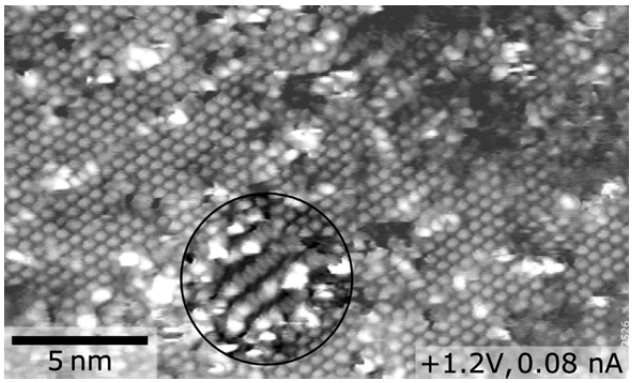

Figure 3. Small area of the (2 × 1) reconstruction after liquid H_2O exposure. Ridges and valleys of the original (2 × 1)-reconstructed surface (small fraction highlighted by a circle) are aligned with the rows of the restructured surface.

Surface Spectroscopy (XPS and LEIS). Special attention was placed on maintaining sufficiently clean conditions to be able to exclude the possibility of contaminant-induced artifacts. This was verified by characterizing the sample with XPS and LEIS before and after contact with liquid water. Figure 4 shows comparisons of detailed XPS regions of the O 1s, Ti 2p, and C 1s core levels of the UHV-prepared surface and the surface after having been in contact with liquid water. There is a small high-binding-energy shoulder in the O 1s peak corresponding to a dissociated water (OH) peak at 532.1 eV. The OH shoulder is more pronounced in grazing emission (60° from surface normal) and indicates the presence of dissociated water at the surface. The small decrease at 457 eV in the Ti 2p spectrum upon exposure to liquid water (marked with an arrow) is consistent with an oxidation of Ti^{x+} ($x < 4$) defect species to Ti^{4+}. While the C 1s spectrum in Figure 4c, acquired in normal emission, is almost identical to that of the clean surface, the spectrum in Figure 4d, acquired in grazing emission for higher surface sensitivity, shows a minor increase in adventitious carbon (binding energy of 284.2 eV) and a smaller, second peak at 288.5 eV. Reference 11 has attributed a similar C 1s peak at 289 eV to bicarbonate on TiO_2 rutile (110) which forms spontaneously in the ambient environment. Apart from this minor increase of carbon signal no impurities were detected upon the water drop exposure (see the Supporting Information for an XPS overview).

For a quantitative estimate of C contamination, we prepared a saturation coverage (0.5 ML) of formate ($HCOO^-$) on the TiO_2 rutile (110) surface by dosing excess HCOOH in UHV. Formic acid adsorbs dissociatively on TiO_2 (110) at room temperature and forms a dense (2 × 1) layer containing one carbon atom every two Ti 5c surface atoms (1/2 carbon atom per unit cell).[28] On such a surface a reference XPS spectrum with the same system and settings was acquired. By comparing the spectra in Figure 4c, the carbon contamination of the liquid water experiment could be quantified to be below 0.10 ML.

A pseudohexagonal structure that somehow resembles the one in Figure 2a has been observed in ref 29. Such a structure was attributed to Ca impurities segregating from crystal bulk[30] or intentionally prepared as mixed oxide monolayer by depositing metals (Fe, Cr, Ni, V) in oxidizing atmosphere.[31] In order to address the possible presence of such impurities, we complemented the XPS measurements with LEIS—a method that provides an extremely high sensitivity to the composition of the topmost atomic layer. On the UHV-prepared surface only the O (mass 16) and Ti (mass 48) peaks were detected (see Figure 5). No foreign elements were detected by LEIS also after contact with liquid water.

On the basis of these spectroscopic data, we can infer that there are no conspicuous impurities at the surface after contact with liquid water and that the observed overlayer is composed of dissociated water on the TiO_2 surface.

Computational Results. Figures 6a and 6b show the bulk (1 × 1) termination with the lowest-energy arrangements of two dissociated water molecules per (2 × 1) unit cell (dissociative adsorption is 0.11 eV per water molecule more favorable than molecular adsorption). A total of 18 different arrangements were tested (see Supporting Information); all other cases were more than 0.22 eV higher in energy (per (2 × 1) unit cell). The structure in Figure 6a is 0.05 eV higher in energy than the one in Figure 6b, which is due to the fact that the latter forms an additional H bond per OH group. However, the absence of this additional H bond increases the degrees of freedom of the structure depicted in Figure 6a and thereby its entropy. This structure is thus expected to be entropically favored at finite temperature. The thermal motion of the terminal H is also taken into account when simulating STM images. At finite temperature STM is expected to produce an average of the various possible configurations; the simulated images in Figures 6a,b are obtained from averaging over structures in a 4 ps MD run. From the calculated STM images it is apparent that both the reconstructed structure in Figure 1d and the configuration in Figure 6b are predicted to show as rows, whereas the configuration in Figure 6a has a hexagonal-like appearance, where mostly OH groups contribute to the contrast.

DISCUSSION

The requirement that the observed structure has to form on top of the (1 × 1) surface is already evident from the STM image (Figure 2a). The neighboring rows of the observed "c(2 × 1)" structure are imaged as equivalent except for the half-unit-cell shift along the row. This is also demonstrated by the extinctions in the FFT (Figure 2b). Unlike the (2 × 1) reconstruction with its alternating valleys and ridges, the (1 × 1) surface provides a sufficient density of equivalent adsorption sites. Despite this precondition, a number of OH arrangements on top of the (2 × 1) reconstruction were tried computationally. None of them, however, had the right symmetry and density matching the STM observation.

The structure observed by STM (Figure 2a) agrees well with the simulated STM image in Figure 6a. Here, the hydroxyl groups are bound to 5-fold-coordinated Ti surface atoms of the (1 × 1) surface and form an overlayer with a (2 × 1) symmetry. The superstructure, with two OH groups per unit cell, has a glide reflection present along the $[01\bar{1}]$ direction and can be classified as *pg* according to 2D symmetry groups.

DOI: 10.1021/acs.jpcc.7b09674
J. Phys. Chem. C 2017, 121, 26424−26431

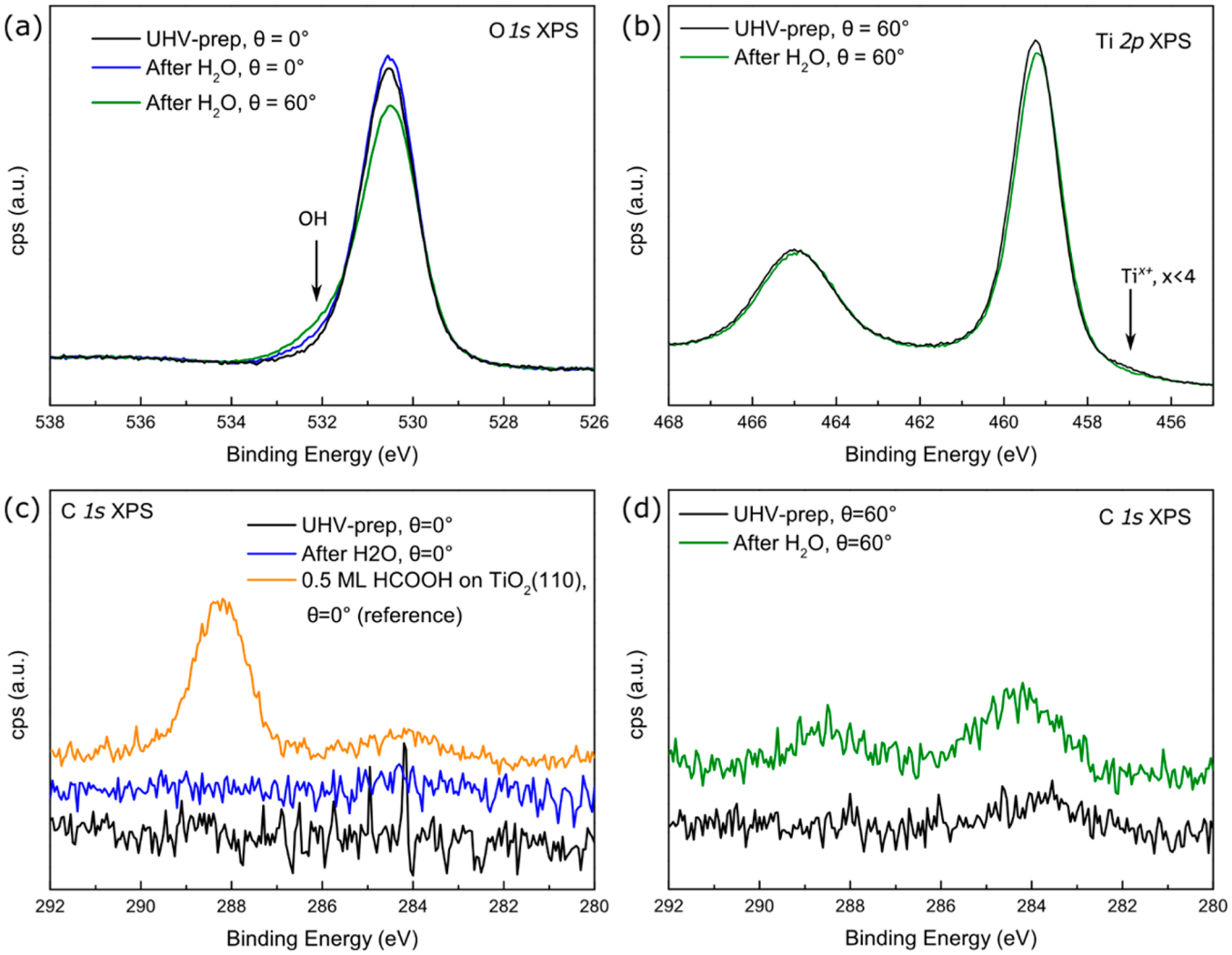

Figure 4. XPS of UHV-prepared TiO_2 rutile (011) and after liquid H_2O exposure. The higher-binding-energy shoulder of the O 1s peak (a) is due to the presence of dissociated water on the surface. A minor increase of the signal in C 1s region (c, d) is attributed to backstreaming of air in the argon flow. Quantitative comparison with the reference spectrum yields an estimate of carbon contamination following the liquid-water experiment to be less than 0.10 ML. All the spectra were normalized to the low-binding-energy background. The individual C 1s spectra in (c) and (d) are vertically offset for clarity.

Comparison of LEED and STM. Contrary to LEED, which averages over the first few atomic layers, STM probes only the topmost atoms on the surface. A (2 × 1) LEED pattern (Figure 2c) is observed for the (2 × 1) OH overlayer on top of the (1 × 1) surface. Although the $[01\bar{1}]$-oriented rows of OH groups are not exactly equidistant, the simulated STM image (Figure 6a) shows almost equidistant rows of protrusions. While the OH groups in the neighboring rows are pointing in different directions, they are at the same height, which leads to the apparent "c(2 × 1)" symmetry and a smaller diamond-shape cell of the OH groups (see Figure 7b). This apparent higher symmetry observed by STM is responsible for the extinction of half the (2 × 1) spots in the FFT of the STM image (Figure 2b).

Domains: Spot Splitting. As observed by STM (Figure 2a), there are domains within the OH overlayer. The domains are separated by domain boundaries that appear as brighter rows along the $[01\bar{1}]$ direction in STM (see Figure 2a). The structure calculated in Figure 6b could well represent the local structure of such an antiphase domain boundary; as the density of OH is locally higher compared to the domain, it can be classified as a heavy domain wall.[32,33] The width of the domains is not fully uniform and can vary with experimental parameters; slightly bigger domains (seven rows in width) were observed in another experiment. The small domains observed in Figure 2a and the resulting high density of domain walls increase the overall coverage of hydroxyls.

The typical domain width in Figure 2a is five rows (ca. 23 Å) and thus smaller than the coherence length of the electron beam (in the range of ∼100 Å).[34] Antiphase domains diffract coherently, which leads to characteristic effects, including splitting of some beams, in the diffraction pattern.[35] Since the antiphase boundaries are parallel and regularly spaced, a splitting of these beams takes place in the direction perpendicular to the orientation of the boundaries.

The general features can be obtained by considering two subdomains of identical dimensions.[35] The interference function for this arrangement contains a modulating function, which depends on the vector **d** connecting the two subdomains (see Figure 7). The vector $\mathbf{d} = d_1\mathbf{a}_1 + d_2\mathbf{a}_2$, where $\mathbf{a}_1$ and $\mathbf{a}_2$ are the lattice base vectors of the (1 × 1) substrate, determines the phase shift between scattered electrons from the neighboring

DOI: 10.1021/acs.jpcc.7b09674
J. Phys. Chem. C 2017, 121, 26424−26431

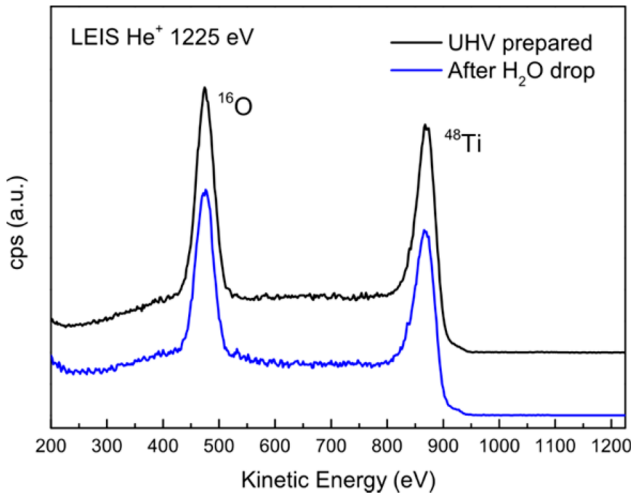

Figure 5. LEIS of UHV-prepared TiO_2 rutile (011) and after liquid H_2O exposure. No impurities were detected either on the UHV-prepared surface or after the contact with liquid water. The spectra are vertically offset for clarity.

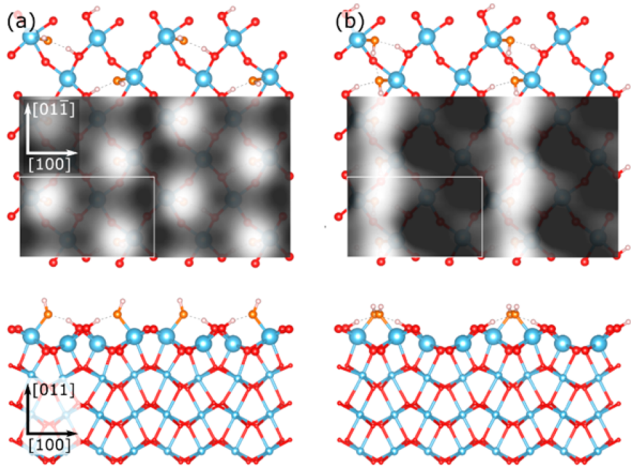

Figure 6. Calculated structures of the hydroxylated (1 × 1) surface as observed after exposure to liquid water. Top views and side views of (a) the bulk-terminated (1 × 1) surface with two water molecules per (2 × 1) unit cell dissociatively adsorbed in different trenches and (b) the (1 × 1) surface with two dissociatively adsorbed water molecules in the same trench. Oxygen atoms belonging to terminal OH groups are highlighted in orange, and the white rectangle in the STM images shows the unit cell used for the calculations. STM images are computed for a 0.5 eV bias from the conduction-band minimum and a 10^{-6} e/Å^3 isodensity. The STM images are obtained by averaging STM images of a Born−Oppenheimer MD at 300 K. All of the displayed underlying atomic structures are the fully relaxed ones.

domains. Beam splitting occurs when one of the diffraction maxima of the perfect surface coincides with a minimum of the modulating function. This condition is satisfied when

$$hd_1 + kd_2 = \frac{1}{2}(2n + 1) \quad (1)$$

where h and k are indices of the diffracted beams, d_1 and d_2 are components of the connecting vector **d**, and n is an integer number.

Figure 7 shows a model of (1 × 1) surface of TiO_2 rutile (011) with two antiphase domains of the (2 × 1) OH overlayer on top (as in Figure 6a). The domains are separated by a

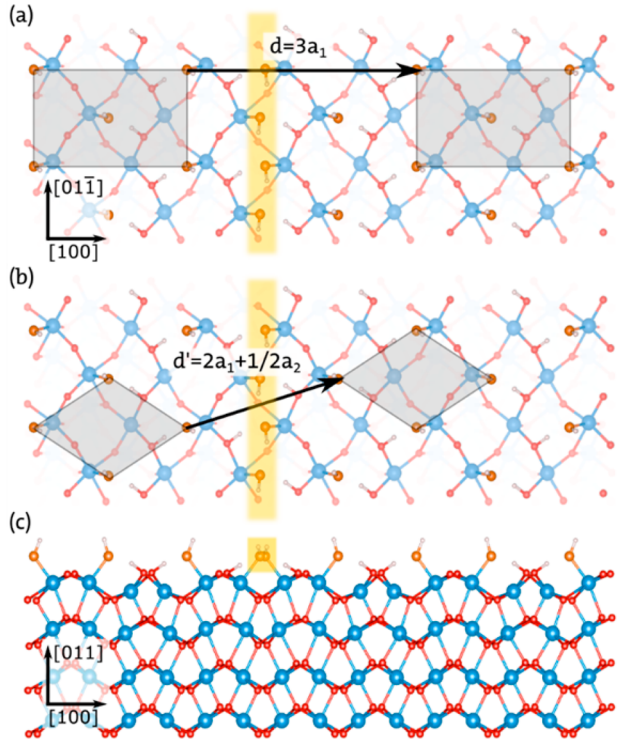

Figure 7. Antiphase domains within the OH overlayer on top of (1 × 1) surface. (a) The structure with a highlighted (2 × 1) unit cell, (b) the structure with a highlighted apparent "c(2 × 1)" unit cell as seen by STM, and (c) section view. The vectors **d** and **d′** connect the unit cells across the domain boundary.

domain boundary (calculated structure in Figure 6b). In Figure 7a, two equivalent (2 × 1) unit cells across the domain boundary are highlighted with a rectangle. The connecting vector across the domain boundary can be expressed as $\mathbf{d} = 3\mathbf{a}_1 + 0\mathbf{a}_2$. By substituting this vector, eq 1 becomes $6h = 2n + 1$. Therefore, only the half-order beams (where h is a fractional number) fulfill the condition. Only the fractional spots are split, in agreement with the experimental LEED pattern (Figure 2c). If the domains formed on top of the original (2 × 1) reconstructed surface, which has negligible density of domain boundaries, the half-order spots would be sharp.

The different perception of the structure by LEED and the FFT results in different connecting vectors across the domain boundary. The two differently oriented OHs per (2 × 1) unit cell are not discriminated by STM, which leads to an apparent diamond-shape unit cell (highlighted in Figure 7b). The two nearest "c(2 × 1)" unit cells are now connected by a different vector, $\mathbf{d}' = 2\mathbf{a}_1 + {}^1/_2\mathbf{a}_2$. As the equation above becomes $4h + k = 2n + 1$, only the (h, k) spots with odd k-index will be split. This is again in agreement with observed spot-splitting in the FFT in Figure 2b. In fact, this description points again at the spots with fractional value of h-index. In the reciprocal pattern of the "c(2 × 1)", all the present spots with odd k-index have a fractional h-index (and vice versa).

Proposed Mechanism. On the basis of our experimental results and DFT calculations, we propose the following mechanism occurring on the TiO_2(011) surface in liquid-water environment. The (2 × 1) reconstruction of the UHV-prepared surface is lifted when the surface is in contact with liquid water, as predicted in ref 19. The deconstruction is achieved by rearranging only the surface atoms, and there is no

DOI: 10.1021/acs.jpcc.7b09674
J. Phys. Chem. C 2017, 121, 26424−26431

mass transport involved. After evacuation of the liquid water, dissociated water remains adsorbed on terminal, undercoordinated Ti 5c atoms of the (1 × 1) surface. These hydroxyls form an ordered overlayer with (2 × 1) symmetry and two hydroxyl groups per unit cell.

The results reported here are distinctly different from those reported in the literature in the case of vapor-phase water dosed on the sample at low temperature, where 1D water chains along the $[01\bar{1}]$ direction were observed on top of the (2 × 1) reconstruction.[36,37] At low temperature, dense layers can be formed but the activation energy required to lift the reconstruction, dissociate water molecules, and form an ordered structure cannot be overcome. On the other hand, at room temperature, the gas-phase water adsorbs mainly on the surface defects but does not form dense layers under the low-pressure conditions of a UHV experiment.

It is well-known that the presence of adsorbates often changes the surface structure. For TiO_2(110) it was shown recently[20] that the substantial relaxations of the clean surface are lifted upon adsorption of methanol, which in turn affects the interaction between neighboring adsorbed molecules. A similar effect was postulated to occur for acetic acid adsorption on TiO_2(011), where weak interaction was observed on the (2 × 1) surface under UHV conditions,[21] but one-dimensional clusters formed at higher exposures. Interestingly, exposure to water vapor at relatively high pressures (10^{-3} mbar) showed similar one-dimensional rows.[21] In contrast to the work presented here, no chemical analysis was provided. One challenge with high-pressure experiments is possible contaminants, which were carefully avoided in the present work. The complete lifting of the reconstruction in an aqueous environment, as first postulated based on DFT calculations,[19] can thus be confidently considered as confirmed, with the additional observation that the unreconstructed surface will be covered with dissociated water.

SUMMARY AND CONCLUSION

The TiO_2 rutile (011)-(2 × 1) surface was prepared and characterized in UHV. The surface was then exposed to liquid water and after evacuation of remaining water characterized again in UHV. A restructuring upon contact with liquid H_2O at room temperature was observed. In line with theoretical predictions,[19] the surface deconstructed into a bulk-terminated (1 × 1) surface. On top of the (1 × 1) surface an ordered overlayer of dissociated water formed with a (2 × 1) symmetry containing two hydroxyl groups per unit cell. In STM, an apparent higher "c(2 × 1)" symmetry was observed. XPS and LEIS measurements excluded restructuring due to contaminants.

The results reported here differ from the studies of gas-phase water adsorption on the same surface reported in the literature. The TiO_2 rutile (011) is an exemplary system where surface-science studies closer to real conditions are needed to be able to transfer the knowledge into applications.

ASSOCIATED CONTENT

Supporting Information

The Supporting Information is available free of charge on the ACS Publications website at DOI: 10.1021/acs.jpcc.7b09674.

XPS overview spectra, LEED pattern showing spots splitting at 50 eV; STM, LEED, and LEIS data of formation of mixed oxide on rutile TiO_2(011) surface due to segregation of Mg impurities and DFT results for additional OH adsorption configurations on the (1 × 1) termination (PDF)

AUTHOR INFORMATION

Corresponding Author

*E-mail diebold@iap.tuwien.ac.at; Tel +43-(0)1-58801-13425.

ORCID

Ulrich Aschauer: 0000-0002-1165-6377
Stijn F. L. Mertens: 0000-0002-5715-0486
Annabella Selloni: 0000-0001-5896-3158
Ulrike Diebold: 0000-0003-0319-5256

Notes

The authors declare no competing financial interest.

ACKNOWLEDGMENTS

This work was supported by an Advanced Grant from the European Research Council European Research Council ("OxideSurfaces" ERC-2011-ADG_20110209), the Austrian Science Fund FWF (Wittgenstein prize Z 250-N27, and Doctoral College "Solids4Fun" W1243-N16). U.A. was supported by the SNF Professorship Grant PP00P2_157615. A.S. acknowledges support by DoE-BES, Division of Chemical Sciences, Geosciences and Biosciences, under Award DE-FG02-12ER16286. Calculations were performed on UBELIX (http://www.id.unibe.ch/hpc), the HPC cluster at the University of Bern.

REFERENCES

(1) Thiel, P. A.; Madey, T. E. The Interaction of Water with Solid-Surfaces - Fundamental-Aspects. *Surf. Sci. Rep.* **1987**, *7*, 211−385.

(2) Henderson, M. A. The Interaction of Water with Solid Surfaces: Fundamental Aspects Revisited. *Surf. Sci. Rep.* **2002**, *46*, 1−308.

(3) Hodgson, A.; Haq, S. Water Adsorption and the Wetting of Metal Surfaces. *Surf. Sci. Rep.* **2009**, *64*, 381−451.

(4) Michaelides, A.; Ranea, V. A.; de Andres, P. L.; King, D. A. General Model for Water Monomer Adsorption on Close-Packed Transition and Noble Metal Surfaces. *Phys. Rev. Lett.* **2003**, *90*, 90.

(5) Michaelides, A.; Morgenstern, K. Ice Nanoclusters at Hydrophobic Metal Surfaces. *Nat. Mater.* **2007**, *6*, 597−601.

(6) Carrasco, J.; Hodgson, A.; Michaelides, A. A Molecular Perspective of Water at Metal Interfaces. *Nat. Mater.* **2012**, *11*, 667−674.

(7) Mugarza, A.; Shimizu, T. K.; Cabrera-Sanfelix, P.; Sanchez-Portal, D.; Arnau, A.; Salmeron, M. Adsorption of Water on O(2 × 2)/Ru(0001): Thermal Stability and Inhibition of Dissociation. *J. Phys. Chem. C* **2008**, *112*, 14052−14057.

(8) Mu, R. T.; Zhao, Z. J.; Dohnalek, Z.; Gong, J. L. Structural Motifs of Water on Metal Oxide Surfaces. *Chem. Soc. Rev.* **2017**, *46*, 1785−1806.

(9) Diebold, U. The Surface Science of Titanium Dioxide. *Surf. Sci. Rep.* **2003**, *48*, 53−229.

(10) Hussain, H.; Tocci, G.; Woolcot, T.; Torrelles, X.; Pang, C. L.; Humphrey, D. S.; Yim, C. M.; Grinter, D. C.; Cabailh, G.; Bikondoa, O.; et al. Structure of a Model TiO_2 Photocatalytic Interface. *Nat. Mater.* **2016**, *16*, 461−466.

(11) Song, A. Q.; Skibinski, E. S.; DeBenedetti, W. J. I.; Ortoll-Bloch, A. G.; Hines, M. A. Nanoscale Solvation Leads to Spontaneous Formation of a Bicarbonate Monolayer on Rutile (110) under Ambient Conditions: Implications for CO_2 Photoreduction. *J. Phys. Chem. C* **2016**, *120*, 9326−9333.

(12) Sasahara, A.; Tomitori, M. An Atomic-Scale Study of TiO_2(110) Surfaces Exposed to Humid Environments. *J. Phys. Chem. C* **2016**, *120*, 21427−21435.

(13) Serrano, G.; Bonanni, B.; Di Giovannantonio, M.; Kosmala, T.; Schmid, M.; Diebold, U.; Di Carlo, A.; Cheng, J.; VandeVondele, J.; Wandelt, K.; Goletti, C.; et al. Molecular Ordering at the Interface between Liquid Water and Rutile TiO_2(110). *Adv. Mater. Interfaces* **2015**, *2*, 1500246.
(14) Müllner, M.; Balajka, J.; Schmid, M.; Diebold, U.; Mertens, S. F. L. Self-Limiting Adsorption of WO_3 Oligomers on Oxide Substrates in Solution. *J. Phys. Chem. C* **2017**, *121*, 19743−19750.
(15) Ramamoorthy, M.; Vanderbilt, D.; Kingsmith, R. D. 1st-Principles Calculations of the Energetics of Stoichiometric TiO_2 Surfaces. *Phys. Rev. B: Condens. Matter Mater. Phys.* **1994**, *49*, 16721−16727.
(16) Ohno, T.; Sarukawa, K.; Matsumura, M. Crystal Faces of Rutile and Anatase TiO_2 Particles and Their Roles in Photocatalytic Reactions. *New J. Chem.* **2002**, *26*, 1167−1170.
(17) Torrelles, X.; Cabailh, G.; Lindsay, R.; Bikondoa, O.; Roy, J.; Zegenhagen, J.; Teobaldi, G.; Hofer, W. A.; Thornton, G. Geometric Structure of TiO_2(011)(2 × 1). *Phys. Rev. Lett.* **2008**, *101*, 101.
(18) Gong, X. Q.; Khorshidi, N.; Stierle, A.; Vonk, V.; Ellinger, C.; Dosch, H.; Cheng, H. Z.; Selloni, A.; He, Y. B.; Dulub, O.; et al. The 2 × 1 Reconstruction of the Rutile TiO_2(011) Surface: A Combined Density Functional Theory, X-Ray Diffraction, and Scanning Tunneling Microscopy Study. *Surf. Sci.* **2009**, *603*, 138−144.
(19) Aschauer, U.; Selloni, A. Structure of the Rutile TiO_2(011) Surface in an Aqueous Environment. *Phys. Rev. Lett.* **2011**, *106*, 166102.
(20) Silber, D.; Kowalski, P. M.; Traeger, F.; Buchholz, M.; Bebensee, F.; Meyer, B.; Wöll, C. Adsorbate-Induced Lifting of Substrate Relaxation Is a General Mechanism Governing Titania Surface Chemistry. *Nat. Commun.* **2016**, *7*, 12888.
(21) Cuan, Q.; Tao, J. G.; Gong, X. Q.; Batzill, M. Adsorbate Induced Restructuring of TiO_2(011)-(2 × 1) Leads to One-Dimensional Nanocluster Formation. *Phys. Rev. Lett.* **2012**, *108*, 106105.
(22) Choi, J. I. J.; Mayr-Schmölzer, W.; Mittendorfer, F.; Redinger, J.; Diebold, U.; Schmid, M. The Growth of Ultra-Thin Zirconia Films On Pd_3Zr(0001). *J. Phys.: Condens. Matter* **2014**, *26*, 225003.
(23) Giannozzi, P.; et al. Quantum Espresso: A Modular and Open-Source Software Project for Quantum Simulations of Materials. *J. Phys.: Condens. Matter* **2009**, *21*, 395502.
(24) Perdew, J. P.; Burke, K.; Ernzerhof, M. Generalized Gradient Approximation Made Simple. *Phys. Rev. Lett.* **1996**, *77*, 3865−3868.
(25) Vanderbilt, D. Soft Self-Consistent Pseudopotentials in a Generalized Eigenvalue Formalism. *Phys. Rev. B: Condens. Matter Mater. Phys.* **1990**, *41*, 7892−7895.
(26) Tersoff, J.; Hamann, D. R. Theory and Application for the Scanning Tunneling Microscope. *Phys. Rev. Lett.* **1983**, *50*, 1998−2001.
(27) Woolcot, T.; Teobaldi, G.; Pang, C. L.; Beglitis, N. S.; Fisher, A. J.; Hofer, W. A.; Thornton, G. Scanning Tunneling Microscopy Contrast Mechanisms for TiO_2. *Phys. Rev. Lett.* **2012**, *109*, 156105.
(28) Chambers, S. A.; Henderson, M. A.; Kim, Y. J.; Thevuthasan, S. Chemisorption Geometry, Vibrational Spectra, and Thermal Desorption of Formic Acid on TiO_2(110). *Surf. Rev. Lett.* **1998**, *5*, 381−385.
(29) Tao, J. G.; Luttrell, T.; Batzill, M. A Two-Dimensional Phase of TiO_2 with a Reduced Bandgap. *Nat. Chem.* **2011**, *3*, 296−300.
(30) Dulub, O.; Di Valentin, C.; Selloni, A.; Diebold, U. Structure, Defects, and Impurities at the Rutile TiO_2(011)-(2 × 1) Surface: A Scanning Tunneling Microscopy Study. *Surf. Sci.* **2006**, *600*, 4407−4417.
(31) Halpegamage, S.; Wen, Z. H.; Gong, X. Q.; Batzill, M. Monolayer Intermixed Oxide Surfaces: Fe, Ni, Cr, and V Oxides on Rutile TiO_2(011). *J. Phys. Chem. C* **2016**, *120*, 14782−14794.
(32) Oura, K.; Lifshits, V. G.; Saranin, A. A.; Zotov, A. V.; Katayama, M. *Surface Science: An Introduction*; Springer: Berlin, 2003.
(33) Heinz, K.; Starke, U. In *Surface and Interface Science*; Wandelt, K., Ed.; Wiley-VCH: Weinheim, 2012; Vol. 2, pp 489−569.
(34) Van Hove, M. A.; Weinberg, W. H.; Chan, C. M. *Low-Energy Electron Diffraction: Experiment, Theory, and Surface Structure Determination*; Springer-Verlag: Berlin, 1986.
(35) Estrup, P. J.; McRae, E. G. Surface Studies by Electron Diffraction. *Surf. Sci.* **1971**, *25*, 1−52.
(36) He, Y. B.; Li, W. K.; Gong, X. Q.; Dulub, O.; Selloni, A.; Diebold, U. Nucleation and Growth of 1D Water Clusters on Rutile TiO_2 (011)-2 × 1. *J. Phys. Chem. C* **2009**, *113*, 10329−10332.
(37) Di Valentin, C.; Tilocca, A.; Selloni, A.; Beck, T. J.; Klust, A.; Batzill, M.; Losovyj, Y.; Diebold, U. Adsorption of Water on Reconstructed Rutile TiO_2(011)-(2 × 1): Ti = O Double Bonds and Surface Reactivity. *J. Am. Chem. Soc.* **2005**, *127*, 9895−9903.

DOI: 10.1021/acs.jpcc.7b09674
J. Phys. Chem. C 2017, 121, 26424−26431